



Carbazole-based fluorescent probes for G-quadruplex DNA targeting with superior selectivity and low cytotoxicity

Quan-Qi Yu, Ming-Qi Wang*

School of Pharmacy, Jiangsu University, Zhenjiang 212013, PR China

ARTICLE INFO

Keywords:

G-quadruplex DNA
Fluorescent probe
Carbazole
Cell imaging
Cytotoxicity

ABSTRACT

G-quadruplex DNA plays a very important role in clinical diagnosis and fluorescence analysis has attracted extensive attention. A class of carbazole-based fluorescent probes for the detection of G-quadruplex DNA was established in this work. In this system, the installation of an oligo(ethylene glycol) chain on the scaffold will improve the water-solubility and biocompatibility. The presence of styrene-like different side groups could tune the selectivity toward G-quadruplex DNA binding. Results revealed that the substitution pattern and position gave a great influence on the ability for the discrimination of the G-quadruplex from other DNA structures. Especially, probe E1 bound to G-quadruplex DNA with superior selectivity, which exhibiting almost no fluorescence response in the presence of non-G-quadruplex DNA structures. Comprehensive analyses revealed that E1 could bind both ends of the G-quadruplex, resulting in a significant increase of fluorescence emission intensity. Cellular uptake assay suggested that E1 could pass through membrane and enter living cells with low cytotoxicity.

1. Introduction

Targeting of non-canonical DNA secondary structures such as G-quadruplexes is now considered as an appealing opportunity for clinical diagnosis and development of new chemotherapeutic agents, especially because accumulating evidence has suggested the existence of G-quadruplexes *in vivo*^{1–4}. G-quadruplexes, with distinct and various structural features, are four-stranded nucleic acid structures formed by the stacking of two or more G-quartets in the presence of metal ions such as K⁺ and Na⁺^{5–7}. Bio-informatics suggests that putative G-quadruplex-forming sequences are abundantly present across the chromosomes and transcriptomes⁸. As an important secondary nucleic acid structure, G-quadruplex has an essential role in protecting the chromosome from fusion, maintaining the stability of genome and controlling the expression of genes at the transcriptional level^{2,9–11}. Therefore, selective detection of G-quadruplex structures would be very important in the understanding of their biological processes. One of the major challenges in targeting G-quadruplexes is the high specificity toward G-quadruplexes over duplex DNAs, because the sequences of G-quadruplex are engulfed in the soupy embrace of duplexes. To address the challenge, much of the recent efforts are aimed towards the development of biophysical tools and techniques^{12–14}. In particular, fluorescence probes, based on the small organic molecules have made

significant contributions due to overwhelming advantages such as rapidity, high selectivity, and sensitivity, low cost, non-invasive detection as well as real-time detectability^{15–18}.

Recently, several classes of small-molecule fluorescent probes with high selectivity for the G-quadruplex over duplex DNA have been developed^{19–24}. Carbazole derivatives are the widely used fluorescence molecules for G-quadruplex DNA targeting probably due to their attractive structural properties as well as high binding affinities^{25–31}. Substitution of the subunits at a suitable position of carbazole core is found to exert excellent optical properties, like BMVC²⁵, CZ-BT²⁶, TO-CZ²⁷, BPBC²⁸, 9E PBIC²⁹ and others. They show significant fluorescence enhancements and higher binding preference to some G-quadruplexes. However, few of them are able to give almost no fluorescence response when binding with duplex DNAs. In addition, intrinsic toxicity also limits their *in vivo* application. Despite much progress, fluorescent probes for the detection of G-quadruplex DNA structures with superior selectivity are rare and still in highly demand.

Oligo (ethylene glycol) (OEG) chains functionalized with fluorescent probes have received significant interest in considering their flexibility, chemical stability, good biocompatibility and limited toxicity properties³². Based on our experience on the design fluorescent probes for specific G-quadruplex DNA^{33,34}, in this work, to obtain efficient, superior selectivity and low toxicity fluorescent probes that can

* Corresponding author.

E-mail address: wmq3415@163.com (M.-Q. Wang).

<https://doi.org/10.1016/j.bmc.2020.115641>

Received 23 May 2020; Received in revised form 1 July 2020; Accepted 5 July 2020

Available online 10 July 2020

0968-0896/ © 2020 Elsevier Ltd. All rights reserved.

be used for G-quadruplex DNA sensing, a series of new fluorescent probes (**E1**, **E2** and **E3**) which are designed on the combination of a triethylene glycol mono methyl side chain in the center of carbazole scaffold and styrene-like different side groups at its 3-position have been developed. Their fluorescence performance on various DNA forms was investigated. The resulting probes have turn-on fluorescent signal enhancements towards G-quadruplex DNAs, which exhibited remarkable differentiation with respect to its structural position and type of the side groups. More importantly, probe **E1** exhibited virtually no fluorescence response to various duplex DNAs and can penetrate into living cell with low cytotoxicity. The detailed binding properties for G-quadruplex DNA were comprehensively assessed through both experimental and modeling studies.

2. Experimental methods

2.1. Materials and instrumentation

The starting precursors used for synthesis of fluorescent probes were supplied by commercial companies. The chemicals were used as received and no purification process was performed. All oligonucleotides were purchased from Sangon Biotechnology Co., Ltd. (Shanghai, China) and were dissolved in 10 mM Tris-HCl buffer (containing 60 mM KCl, pH 7.4). The sequences were listed in **Table S1**. DNA secondary structures were confirmed by CD spectra (**Fig. S1**). High resolution mass spectra (HRMS) were recorded on a Shimadzu LCMS-IT-TOF instrument with an ESI detector. TEM were carried out on a JEM 2100F field emission transmission electron microscope. Stock solution of probes **E1**, **E2** and **E3** (1 mM) were prepared in DMSO and stored at 4 °C.

2.2. Synthesis and characterization of probes

The synthetic route of the final probes was depicted in **Scheme S1**.

2.2.1. Preparation of 9-(2-(2-(2-methoxyethoxy)ethoxy)ethyl)-9H-carbazole-3-carbaldehyde (intermediate compound **4**)³⁵

POCl₃ (0.89 mL, 1 mmol) was added into DMF (7 mL, 90.8 mmol) under the condition of ice water and the mixture was stirred vigorously for 1 h. Then 9-(2-(2-(2-methoxyethoxy)ethoxy)ethyl)-9H-carbazole (3.1 g, 3 mmol) dissolved in 1, 2-dichloroethane was added into the mixture refluxed overnight under the protection of nitrogen. After cooling to room temperature, Sodium bicarbonate solution was poured into the solution to neutralize the acidity and then extracted with dichloromethane. The solvent was dried with anhydrous sodium sulfate and evaporated on a rotary evaporation. The crude product was purified on a silica gel column eluting with CH₂Cl₂/CH₃OH yielding 0.8 g (yield 32%) of the desired product. ¹H NMR (400 MHz, CDCl₃) δ: 10.06 (s, 1H), 8.56 (d, *J* = 1.2 Hz, 1H), 8.37–7.86 (m, 3H), 7.75–7.10 (m, 4H), 4.50 (t, *J* = 5.8 Hz, 2H), 3.87 (t, *J* = 5.8 Hz, 2H), 3.62–3.32 (m, 9H), 3.30 (s, 3H).

2.2.2. Preparation of probe **E1**

A mixture of intermediate 9-(2-(2-(2-methoxyethoxy)ethoxy)ethyl)-9H-carbazole-3-carbaldehyde (**4**, 350 mg, 1 mmol), 1,2-dimethylpyridin-1-ium iodide (**6**, 240 mg, 1 mmol) and 40 mL anhydrous ethanol, followed by 5 drops catalytic piperidine was refluxed for 12 h under nitrogen with stirring. After cooling to room temperature, the solvent was evaporated under reduced pressure and the residue was recrystallized from dichloromethane to afford **E1** (45.8%, 270 mg) as a yellow solid. ¹H NMR (400 MHz, DMSO-*d*₆) δ: 8.83 (d, *J* = 6.2 Hz, 1H),

8.71 (s, 1H), 8.53 (d, *J* = 8.4 Hz, 1H), 8.42 (t, *J* = 7.9 Hz, 1H), 8.18 (dd, *J* = 20.4, 11.8 Hz, 2H), 8.03–7.91 (m, 1H), 7.79 (t, *J* = 6.8 Hz, 1H), 7.74 (d, *J* = 8.6 Hz, 1H), 7.67 (d, *J* = 8.2 Hz, 1H), 7.61 (s, 1H), 7.57 (s, 1H), 7.49 (t, *J* = 7.7 Hz, 1H), 7.28 (t, *J* = 7.5 Hz, 1H), 4.60 (t, *J* = 5.0 Hz, 2H), 4.39 (s, 3H), 3.45 (dd, *J* = 5.7, 3.6 Hz, 2H), 3.41–3.19 (m, 7H), 3.13 (d, *J* = 6.5 Hz, 3H). ¹³C NMR (100 MHz, DMSO-*d*₆) δ: 154.1, 153.4, 147.0, 146.0, 145.0, 144.4, 144.1, 142.4, 141.6, 141.3, 141.2, 141.1, 129.1, 127.5, 127.3, 126.8, 126.6, 126.5, 126.1, 124.9, 124.6, 124.4, 123.1, 122.7, 122.6, 122.4, 122.2, 121.9, 120.9, 120.7, 120.2, 119.8, 117.8, 114.2, 110.8, 110.7, 110.4, 110.4, 71.6, 70.5, 70.4, 70.1, 70.0, 69.3, 58.4, 46.6, 43.4, 43.2; HRMS: (positive mode, *m/z*) calculated 431.2329, found 431.2326 for [M–I]⁺;

2.2.3. Preparation of probe **E2**

This complex was synthesized in a manner identical to that described for complex **E1**, with 1,4-dimethylpyridin-1-ium iodide in place of 1,2-dimethylpyridin-1-ium iodide. The residue after rotary evaporation was purified by column chromatography on silica gel eluting with CH₂Cl₂/CH₃OH to afford **E2** (55.2%, 325 mg) as a yellow solid. ¹H NMR (400 MHz, DMSO-*d*₆) δ: 8.80 (d, *J* = 6.8 Hz, 2H), 8.56 (s, 1H), 8.19 (t, *J* = 10.8 Hz, 4H), 7.86 (dd, *J* = 8.7, 1.3 Hz, 1H), 7.70 (dd, *J* = 23.6, 8.4 Hz, 2H), 7.50 (dd, *J* = 18.2, 12.1 Hz, 2H), 7.27 (t, *J* = 7.4 Hz, 1H), 4.59 (t, *J* = 5.2 Hz, 2H), 4.22 (s, 3H), 3.44 (dd, *J* = 5.8, 3.6 Hz, 2H), 3.42–3.27 (m, 7H), 3.13 (s, 3H). ¹³C NMR (100 MHz, DMSO-*d*₆) δ: 153.5, 145.1, 142.7, 142.2, 141.3, 126.7, 126.7, 126.6, 123.2, 123.1, 122.5, 121.4, 120.7, 120.4, 120.1, 110.9, 110.6, 71.6, 70.5, 70.1, 70.0, 69.3, 58.4, 47.0, 43.3; HRMS: (positive mode, *m/z*) calculated 431.2329, found 431.2326 for [M–I]⁺.

2.2.4. Preparation of probe **E3**

Probe **E3** was prepared by the same method as above but with 1,2-dimethylquinolin-1-ium iodide to give an orange solid (52.4%, 314 mg). ¹H NMR (400 MHz, DMSO) δ: 9.09–8.80 (m, 2H), 8.73–8.38 (m, 3H), 8.24 (dd, *J* = 16.2, 7.8 Hz, 2H), 8.09 (t, *J* = 9.2 Hz, 2H), 8.03–7.80 (m, 2H), 7.70 (dd, *J* = 32.5, 8.4 Hz, 2H), 7.49 (t, *J* = 7.4 Hz, 1H), 7.29 (t, *J* = 7.3 Hz, 1H), 4.57 (d, *J* = 11.5 Hz, 5H), 3.45 (d, *J* = 4.8 Hz, 2H), 3.4–3.28 (m, 6H), 3.29–3.19 (m, 2H), 3.14 (s, 3H). ¹³C NMR (100 MHz, DMSO-*d*₆) δ: 156.5, 149.5, 145.4, 143.2, 142.7, 141.2, 139.2, 134.6, 130.1, 128.6, 128.3, 127.4, 126.8, 126.5, 123.1, 122.7, 122.5, 121.0, 120.8, 120.3, 119.2, 115.7, 110.7, 71.6, 70.5, 70.2, 70.0, 69.2, 58.4, 43.3; HRMS: (positive mode, *m/z*) calculated 481.2486, found 481.2483 for [M–I]⁺.

2.3. Measurements and methodology

The instruments and the experiments used were identical to the one used in the article we reported earlier³⁶. The 2-Ap titration experiment was carried out as following: probe **E1** or hemin were gradually added into the solution containing 2-Ap labeled c-myc G-quadruplex DNA at fixed concentration (2 μM) in 10 mM Tris-HCl buffer, pH 7.4 in the presence of 60 mM KCl. The fluorescence measurement was taken as E_x = 305 nm.

3. Results and discussion

3.1. Probes design and synthesis

The synthesis of final probes was accomplished by the functionalization of carbazole with a 1-methylpyridinium/1-methylquinolinium moiety through vinylic linkages, using a previously reported standard procedure³¹. The conjugated with different side groups at different

positions were introduced for the investigation of the selectivity towards G-quadruplex DNA structures. The incorporation of the positively charged methylpyridine and methylquinoline could enhance the solubility in buffer solutions. Moreover, the presence of OEG chain in probes facilitates their aqueous compatibility and cell permeability for the imaging in live cells. The detailed synthetic procedure was given in **Scheme S1**. Experimental data including ^1H NMR, ^{13}C NMR and HRMS supported their structures (see the [Supplementary Information](#)).

3.2. Selectivity study of synthesized probes towards G-quadruplex DNAs against other nucleic acids

Initially, the spectral properties of the final probes **E1-E3** were listed in **Table S2**. The probes exhibit an absorption maximum in the visible region between 400 and 445 nm and have a large Stokes shift in Tris-HCl buffer solution at pH = 7.4, which indicated that the probes possessed good anti-interference effect and less energy loss property. Compared with chemical structures of the three probes, featured with the incorporation of quinoline ring on the carbazole core, the corresponding wavelength of absorption maximum was red-shifted and the quantum yield was decreased ($\Phi < 0.01$). This observation could be mainly assigned to the more efficient intramolecular charge transfer (ICT) process³¹. The sensing selectivity of the three probes towards G-quadruplex DNAs was then investigated and evaluated by using fluorescence titrations with different DNA structures including G-quadruplexes, single- and double-stranded DNAs. The changes of the fluorescent spectra obtained during the titration experiments were shown in **Figs. S2-4**. Generally, the new probes induced different levels of fluorescence enhancement upon addition of the DNA structures. Obviously, **E1** that methylpyridine ring connected at its position 2 was perfectly capable of distinguishing G-quadruplex from non-G-quadruplex structures (**Fig. 1**). The enhanced fluorescence intensity of **E1** was found to be remarkable upon binding with different G-quadruplex DNAs (parallel, anti-parallel and hybrid-type), while single- and double-stranded DNAs showed almost no fluorescence enhancement. Interestingly, when the methylpyridine ring connected at its position 4 (**E2**), it responded to most of these DNAs, which gave poor selectivity to G-quadruplex DNA. On the other hand, we found that **E3** which bearing a 2-substituted methylquinoline group instead of methylpyridine moiety also exhibited certain fluorescence response for binding with non-G-quadruplex DNAs. By comparing the fluorescence properties of the three probes, it seems that the structures and positions of substituted group are very crucial to fit the probes with the G-quadruplex DNA structure. Therefore, with the preliminary data from fluorescence titration assays, **E1** displayed the best performance on discriminating G-quadruplex from other single- and double stranded DNAs and was suitable for the research of binding mechanism and cell applications.

3.3. Binding affinities of **E1** with G-quadruplex DNA

We investigated the changes in fluorescence of probe **E1** in the presence of a larger panel of quadruplex DNA structures, as well as single- and double-stranded DNAs, and the representative titration with c-myc G-quadruplex was shown in **Fig. 2A**. In a dilute solution of **E1**, it showed weak fluorescent signal at 547 nm ($\Phi = 0.04$). Upon adding c-myc G-quadruplex DNA, a significantly enhanced emission peak appeared and the signal increased gradually as the concentration of c-myc was increased in the solution ($\Phi = 0.24$). This fluorescent property was also observed when treated with other G-quadruplex DNAs. The fluorescence enhancement might be caused by conformational changes in the excited state of **E1**, most likely by the rotation restriction around the

vinyl-bridge upon its G-quadruplex binding, as clearly shown by the emission enhancement in a viscous medium (**Fig. S5**).

To further ascertain the enhancement of fluorescent signal was due to the specific binding of **E1** with G-quadruplex structure, a competitive assay was carried out in the presence of large amounts of single- and double-stranded DNA with c-myc G-quadruplex DNA (**Fig. 2B**). The enhancement of fluorescent intensity after addition of c-myc G-quadruplex revealed that c-myc was able to displace bound excess ss- and ds-DNA very effectively. Furthermore, to mimic the cellular environment *in vivo*, we used BSA and HSA proteins as interfering biomolecules (**Fig. S6**). The increase of BSA and HSA concentration caused negligible fluorescence change. These findings again demonstrated that **E1** has the promising utility for selective detection of G-quadruplex in the competitive biological environment.

Then, we determined the fluorescence lifetime of **E1** in the absence and presence of the c-myc G-quadruplex DNA ($\lambda_{\text{ex}} = 400$ nm and $\lambda_{\text{em}} = 545$ nm) (**Fig. 2C**). The fluorescence lifetime of free **E1** was calculated as 0.513 ns. In the presence of the c-myc G-quadruplex, the lifetime obviously increased to 3.871 ns. Apparently, the probe **E1** was a G-quadruplex-sensitive probe.

Titration of **E1** with c-myc G-quadruplex was also followed by fluorescence to determine the binding affinity and stoichiometry (**Fig. 2D**). The binding constant was determined as $0.48 \times 10^6 \text{ M}^{-1}$ by an independent-site model³⁷, which also implied the formation of a complex with 1:1 stoichiometry of **E1** and c-myc. Moreover, a Job's plot experiment (**Fig. S7**), which exhibits a maximum at 0.5 fraction of **E1**, further indicated that a 1:1 complex was formed. The detection limit of **E1** for the detection was also an important parameter. The fluorescence titration curve revealed that the fluorescence intensity of **E1** at 545 nm increased linearly with the amount of c-myc G-quadruplex DNA in the 0–0.8 μM range ($R^2 = 0.99$, **Fig. 2D Inset**). Thus, the detection limit was calculated to be 0.18 μM based on the equation $\text{LOD} = 3\sigma/k$ ³⁸. Taken together, such results suggested that **E1** had a potential quantitative sensing ability.

3.4. The effect of **E1** on the conformation and stability of G-quadruplex DNA

The circular dichroism (CD) spectroscopic studies were carried out to assess the structural changes of G-quadruplex DNA upon interaction with probe **E1**. In the presence of K^+ ions, c-myc exhibited a parallel structure, with a positive band at 265 nm and a negative band at 242 nm (**Fig. 3A**). The addition of **E1** to c-myc DNA solution failed to change the locations and intensities of two signal peaks, demonstrating that **E1** did not affect the conformation of c-myc G-quadruplex DNA structure.

Having established that probe **E1** could sense and interact with G-quadruplex DNA structures, we further investigated whether such probe could induce G-rich sequence c-myc into G-quadruplex structure and present obstacles to DNA synthesis by DNA polymerases. For this purpose, the primer extension reaction was initiated by the addition of Taq DNA polymerase to a mixture of 24-mer c-myc G-quadruplex forming sequence and its partial complementary sequence (21-mer). As expected, the reaction performed in the absence of any added ligand generated a full-length product (**Fig. 3B**, lane 1). In theory, if a ligand could transform the G-rich sequence c-myc into G-Quadruplex structure, the primer extension by Taq DNA polymerase would be blocked. It was observed that the inhibitory effect becomes more obvious at high concentration of **E1** (**Fig. 3B**), indicating that **E1** could enhance Taq DNA polymerase suspend the DNA polymerization process by stabilizing the G-quadruplex structure. To further confirm the inhibitory

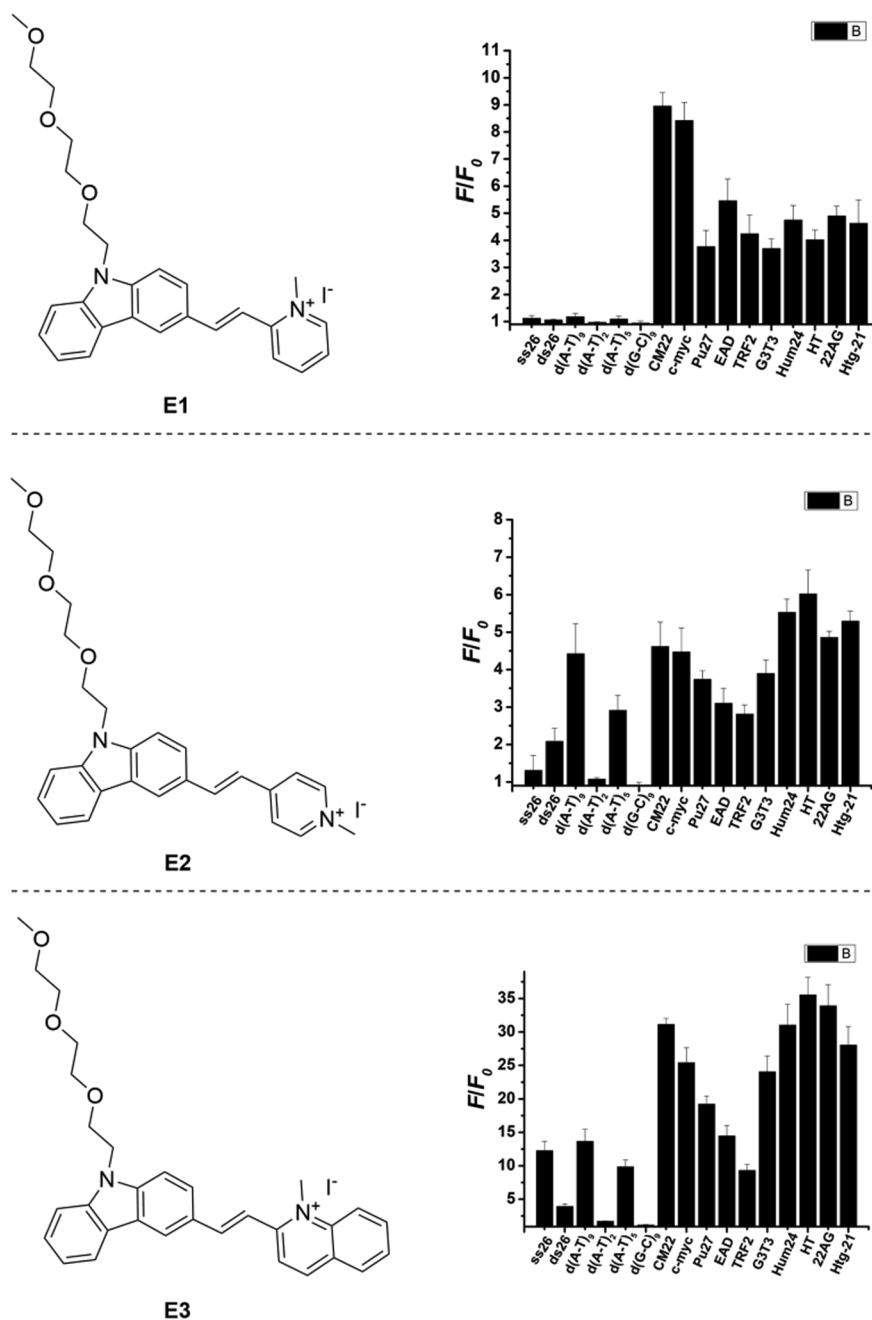


Fig. 1. Comparison of enhancements of emission intensity of **E1**, **E2** and **E3** with single-, and double-stranded DNAs; G-quadruplexes DNAs in 10 mM Tris-HCl buffer (pH 7.4) containing 60 mM KCl. The concentration of each probe was 1 μ M.

effect, a control oligomer, *Mut c-myc*, which cannot form the G-quadruplex structure, was conducted. Under the same conditions, the control oligomer demonstrated no inhibition (Fig. S8). These results further indicated that **E1** was able to stabilize the structures of *c-myc* G-quadruplex DNA, and inhibit in vitro DNA synthesis.

3.5. Study on the binding mechanism of **E1** with *c-myc* G-quadruplex

The above experimental results showed that the probe **E1** was giving excellent fluorescent signal discrimination to G-quadruplex DNA.

In order to get a deep insight into the nature binding of **E1** to G-quadruplex DNA, an elementary and rapid technique, G4/hemin peroxidase inhibition assay^{39,40}, was exploited in this study. The binding modes between G-quadruplex and small molecule usually contain groove binding and end-stacking. Hemin considered as binding to G-quadruplex through end-stacking, could result catalytic activity on the oxidation of ABTS²⁻ by H₂O₂. If **E1**, the candidate ligand, competes with hemin for G-quadruplex binding, will lead to diminish of the catalytic activity of G4/hemin peroxidase, then could be confirmed that it has the same reaction site with G-quadruplex as hemin. As shown in

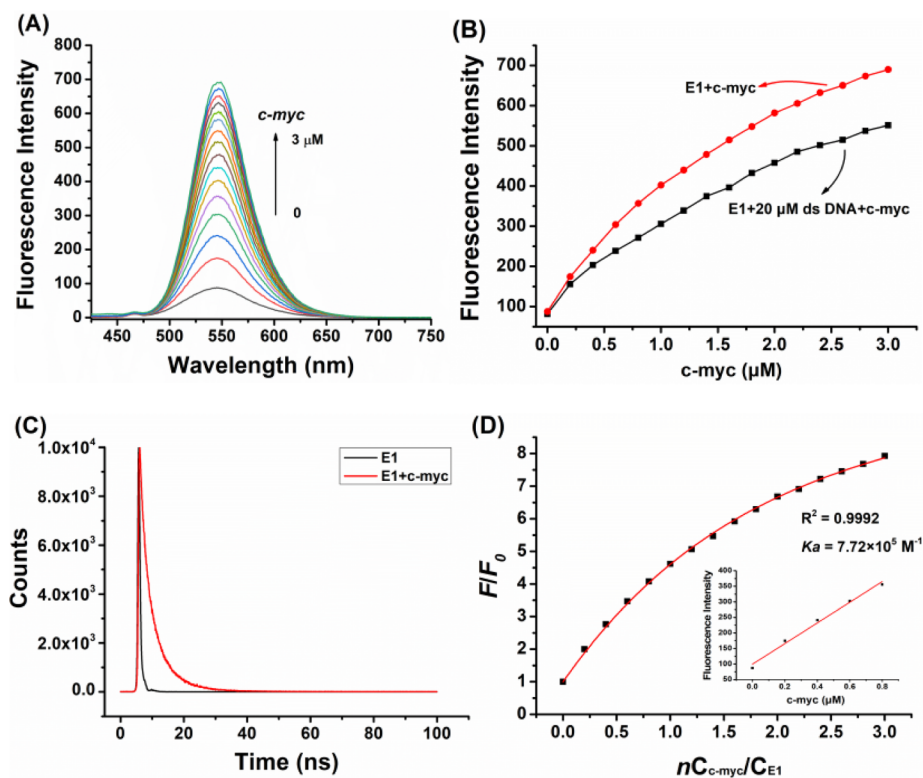


Fig. 2. (A) Fluorescence titration of 1 μM of E1 with stepwise addition of the c-myc G-quadruplex DNA, in 10 mM of Tris-HCl buffer and 60 mM of KCl at a pH of 7.4 (arrows: 0–3 μM). (B) Fluorescence titration of 1 μM of E1 with the stepwise addition of c-myc G-quadruplex DNA with 20 μM ds26 in 10 mM of Tris-HCl buffer and 60 mM of KCl at a pH of 7.4. (C) The fluorescence lifetime decay of E1 without and with c-myc G-quadruplex in 10 mM of Tris-HCl buffer and 60 mM of KCl at a pH of 7.4. (D) Fluorescence titration, presented as a relative increase of the integral fluorescence (F/F_0) of c-myc G-quadruplex DNA with probe E1 (1 μM) in 10 mM of Tris-HCl buffer and 60 mM of KCl at a pH of 7.4. The lines represent fitting to the independent-site model. Inset: Normalized response of the fluorescence signal to changing c-myc G-quadruplex DNA concentrations.

Fig. 4. with addition of different concentrations of E1, the absorbance at 415 nm (oxidized product of ABTS^{2-}) was slightly restrained, indicating that E1 could not compete with hemin by the end-stacking model. Given that, there were two possible conclusions: 1) E1 bound with G-quadruplex DNA with the loops/grooves; 2) E1 gave a low binding affinity at the same site as hemin.

To shed light on the binding mode, mutated c-myc G-quadruplex DNA sequences with different loops were prepared. A fluorescence titration experiment was performed by adding these mutated c-myc sequences to the solution of E1, so as to investigate the influence of these loop regions. As shown in Table 1 and Fig. S9, the extension and shortening of three propeller loop and two flanking loop regions has almost no effect on fluorescence intensity. This result provided evidence that E1 bound to c-myc G-quadruplex DNA may through end-stacking mode rather than groove binding mode.

Molecular docking models were generated by using Autodock Vina modeling tool^{41,42} to investigate the best binding mode between G-quadruplex and ligand. The NMR G-quadruplex structure of c-myc (PDB 217v) was used as the template. Probe E1 could undergo a conformational change upon interaction with G-quadruplex, as it has the rotational flexibility due to vinyl bond between carbazole and pyridyl unlike previous reported structure with large rigid conjugated aromatic groups. From the blind docking results, two possible binding models (end-stacking at the site of 5' terminal and 3' terminal) were selected on the basis of their low energy (Fig. 5). In these models, E1 presented a stretching conformation and covered a large surface area of G-tetrad. In addition, the carbazole moiety exhibited π - π stacking interaction with G-quartet planes to form a complex, allowing effective interaction of triethylene glycol monomethyl ether group and pyridine ring into G-quadruplex groove region, which helped E1 to anchor in the binding

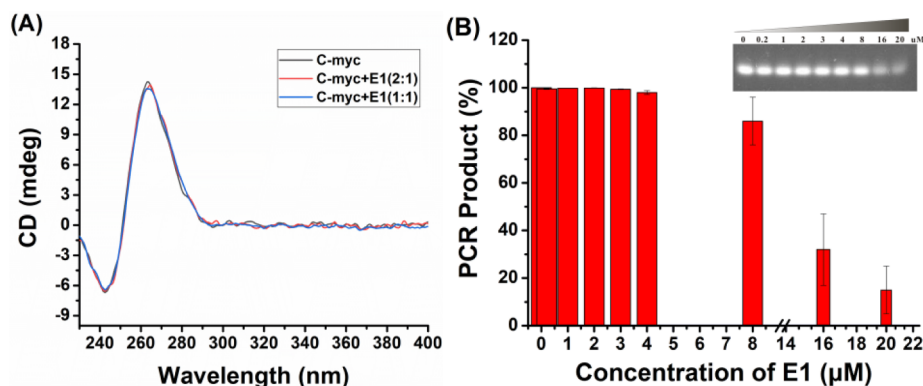


Fig. 3. (A) CD titration spectra of c-myc G-quadruplex DNA (5 μM) with 0–2 equiv E1 in 10 mM Tris-HCl buffer, 60 mM KCl, pH 7.4. (B) Effects of E1 on the PCR-stop assay with c-myc. E1 (0–20 μM) was added to the reaction mixture containing 1x PCR buffer, 10 pmol c-myc, 10 pmol C-myc rev, 0.2 mM dNTPs and 1.5 units of Taq polymerase. The PCR products were separated on 15% non-denaturing polyacrylamide gels in 1 \times TBE.

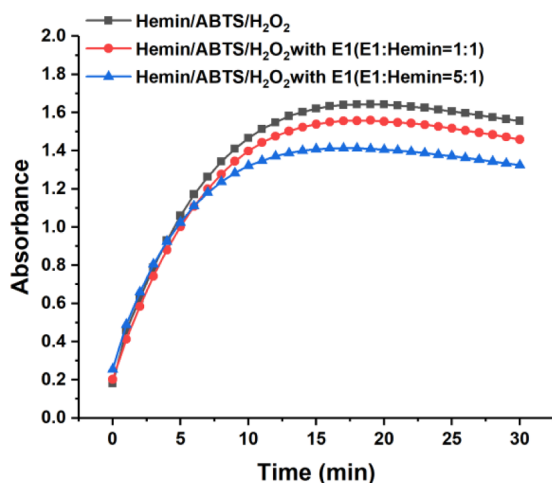


Fig. 4. Inhibition activity of E1 on c-myc G4/hemin complexes in 10 mM Tris-HCl buffer, 60 mM KCl, pH 7.4. Conditions: $[ABTS^{2-}] = 0.18$ mM; $[H_2O_2] = 0.06$ mM; $[c\text{-myc}] = 0.4$ μ M; $[hemin] = 0.8$ μ M; The curves represent the change of the product concentration (absorbance at 415 nm) of G4/hemin peroxidase within 30 min.

Table 1

Relative fluorescence intensities of E1 (1 μ M) in the presence of c-myc G-Quadruplexes (3 μ M) with different flanking loops in 10 mM Tris-HCl buffer, 60 mM KCl, pH 7.4.

Name	Sequence (5'-3')	Relative FI
<i>c-myc</i>	TTGA GGG T GGG TA GGG T GGG TAAA	695
<i>c-myc-1</i>	TTG AATGGG TGGGT AGGGT GGGT AAA	702
<i>c-myc-2</i>	TTG AGGG TAAGGGT AGGGT GGGT AAA	910
<i>c-myc-3</i>	TTG AGGG TGGGT AATGGGT GGGT AAA	632
<i>c-myc-4</i>	TTG AGGG TGGGT AGGGT ATGGGT AAA	570
<i>c-myc-5</i>	TTG AGGG TGGGT AGGGT GGGT AAATA	852
<i>c-myc-6</i>	AGGG TGGGT AGGGT GGGT AAA	846
<i>c-myc-7</i>	TTG AGGG TGGGT AGGGT GGGT	861

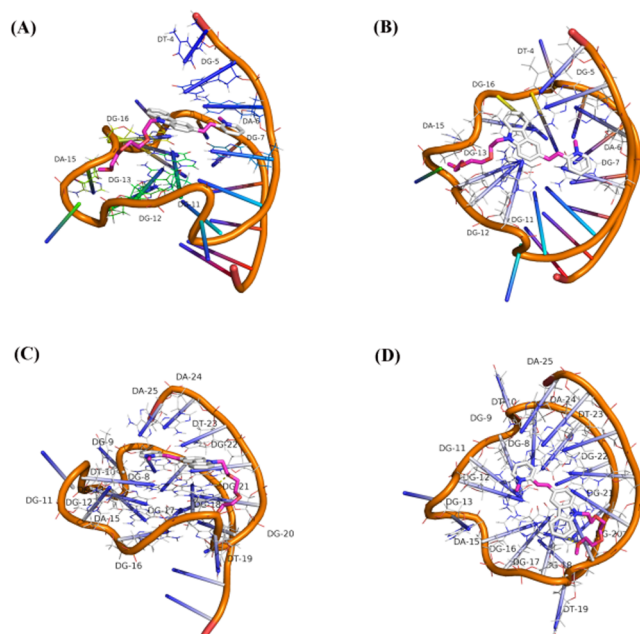


Fig. 5. End-stacking binding modes of E1 to c-myc G-quadruplex DNA by molecular docking. (A) Side view and (B) Top view of E1 binding to 5'-end; (C) Side view and (D) Top view of E1 binding to 3'-end (PDB: 217v).

site of the G-quadruplex DNA. The binding energy in 5' terminal (-6.7 kcal/mol) was equivalent to that in 3' terminal (-6.8 kcal/mol), so the occupation of E1 to each binding site contributes equally.

Modification of 2-aminopurine (2-Ap) in different loops has been widely accepted as a method to study the binding sites between G-quadruplex and binding ligand⁴³. In order to further determine whether the binding site of probe E1 to c-myc G-quadruplex was at the 3' or 5' terminal, we monitored the impact of E1 binding on the modified c-myc G-quadruplex DNA with 2-Ap substituted at position of 4th (Ap4), 13th (Ap13) and 22rd (Ap22) from the 5'-terminus of the c-myc sequence, which were located at 5' terminal, propeller loop region and 3' terminal, respectively. With the resulting emission spectra being shown in Fig. 6, fluorescence intensities of Ap4, Ap13 and Ap22 were all disturbed significantly, indicating that closer interaction occurred among these bases. We further used hemin which is in favor of both 3' and 5'-end stacking of G-quadruplex DNA for comparison³⁹. Under the same experimental conditions, the fluorescence intensities of Ap4, Ap13 and Ap22 in c-myc were also obviously disturbed by hemin. Combined with above results, it seems that E1 had a weak competition with hemin at the same site for G-quadruplex binding. In order to validate the binding mechanism, we carried out a FID assay, in which the ability of hemin to displace the fluorescent probe of E1 from G-quadruplex DNA system. Hemin having the same binding site will compete with E1 for G-Quadruplex binding, resulting in the large decrease of the emission. The data shown in Fig. S10 illustrated that with addition of 1 equiv hemin to the E1-G-Quadruplex DNA system, the almost fully quenched in fluorescence emission was observed, which confirmed the competitive binding of hemin with E1.

3.6. Confocal fluorescence imaging

The most important advantage of fluorescent probes would be intracellular detection. And low cytotoxicity is also one of the most critical requirements for fluorescent probes. Taken the prior results into consideration, it seems that probe E1 has the potential to be applied into the further study of living cell staining and imaging due to its selective enhancement of fluorescence upon binding to G-quadruplex DNA. First, cell viability assays have been performed using CCK-8 method to evaluate the cytotoxicity of E1 towards three cell lines, including two cholangiocarcinoma cell lines (HCCC-9810, RBE) and a non-malignant human cell line (293 T). After three cells exposed to different concentrations of E1 from 0 to 100 μ M for 72 h, the viable cells were quantified, as shown in Fig. S11. It was noteworthy that growth of these cells was not significantly inhibited at a low concentration ($IC_{50} > 40$ μ M), indicating that this probe was safe for bio-imaging in living cells. Thus, the application of E1 as a selective staining agent for the detection and imaging of G-quadruplexes in HCCC-9810 was investigated by using confocal fluorescence microscopy. As for comparison, probes E2 and E3 were also studied. The confocal imaging showed that all of these three probes could enter living cells (Fig. 7). E2 and E3 exhibited higher cellular uptake than E1 based on the fluorescence intensity in cells. The co-staining with nucleus-targeted dye DAPI showed that E1 and E2 with pyridinium arms mainly located in cytoplasm, and E3 with quinolinium arm mainly located in nucleoli. The results of experiment in vitro was not in correspondence with that of experiments in vivo, which may be due to some reasons: 1) G-quadruplex formation in gene occurs transiently when the double-stranded DNA is actively denatured during transcription and replication, the fluorescence of complex upon binding to G-quadruplex might be hardly observed; 2) their diverse affinities to the constituents of the nucleus as well as differences in their photophysical properties; 3) these probes located in a viscosity environment just like they dissolved in ethylene glycol solution. Further we will focus on the modification of these probes and for enhancing their ability of visualizing G-quadruplex DNA structure in living cells.

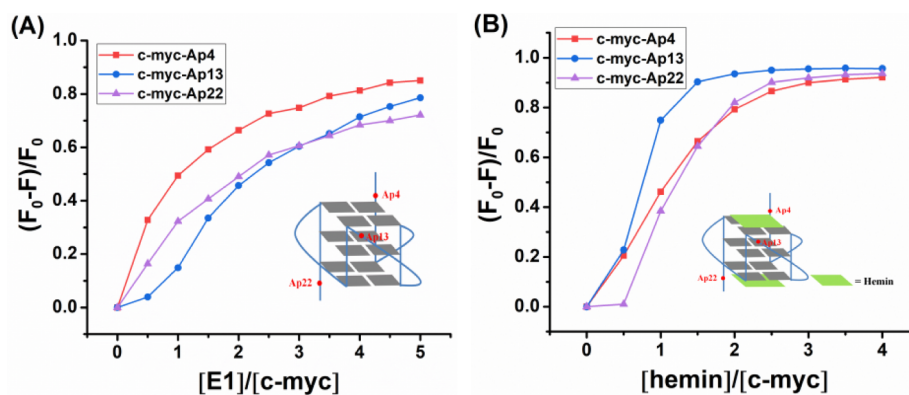


Fig. 6. Plot of $(F_0-F)/F_0$ of 2-Ap individually labelled c-myc G-quadruplex DNA versus binding ratio of $[E1]/[c-myc]$ (A) and $[Hemin]/[c-myc]$ (B), $\lambda_{ex} = 305$ nm, $\lambda_{em} = 368$ nm. Inset: structures model of the parallel G-quadruplex c-myc and hemin. The positions of 2-Ap bases were marked.

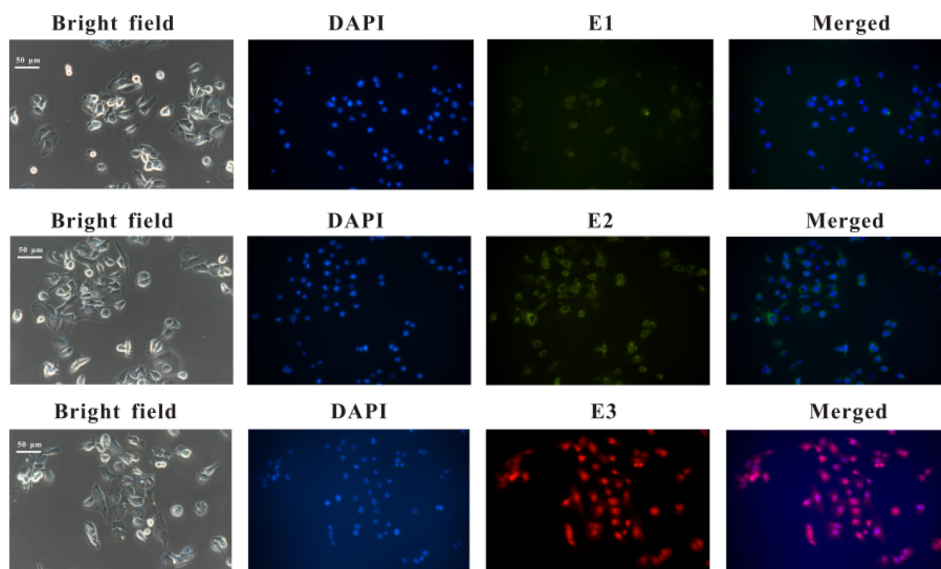


Fig. 7. Confocal fluorescence images of living HCCC-9810 cells stained with 20 μ M E1, E2, E3 and 5 mg/mL DAPI for 0.5 h. Scale bar is 50 μ m.

4. Conclusions

In this work, the Knoevenagel type chemistry has been used to obtain a series of carbazole-based fluorescence probe for the detection of G-quadruplex DNA. We demonstrated that the significance of pyridinium side group and its position when conjugating with the carbazole scaffold through an ethylene bridge in molecular probe design. The fluorescent probe, E1, possessed an excellent selectivity towards G-quadruplex DNA over duplex DNA and other biologically-relevant molecules with fluorescent turn-on signal. The comprehensive binding mechanism studies, together with the molecular modeling analysis indicated that E1 bound with G-quadruplex by the end-stacking model. Furthermore, this probe can enter into living cells and mainly locate in cytoplasm with low cytotoxicity. In fact, there is still a strong need for novel probes that are capable of responding to G-quadruplex DNA structures. The current study highlights the potential of the molecular scaffold of E1 in G-quadruplex selective recognition and gave some crucial factors on developing of effective probes for G-quadruplex DNA applications.

CRediT authorship contribution statement

Quan-Qi Yu: Data curation, Investigation, Formal analysis, Writing - original draft. **Ming-Qi Wang:** Conceptualization, Funding acquisition, Methodology, Project administration, Resources, Supervision,

Validation, Writing - review & editing.

Declaration of Competing Interest

The authors declare that they have no known competing financial interests or personal relationships that could have appeared to influence the work reported in this paper.

Acknowledgements

This work was financially supported by the National Natural Science Foundation of China (21907042), Natural Science Foundation of Jiangsu Province (BK20180857).

Appendix A. Supplementary data

Supplementary data to this article can be found online at <https://doi.org/10.1016/j.bmc.2020.115641>.

References

- Biffi G, Tannahill D, McCafferty J, Balasubramanian S. Quantitative visualization of DNA G-quadruplex structures in human cells. *Nat Chem.* 2013;5:182–186.
- Rhodes D, Lipps HJ. G-quadruplexes and their regulatory roles in biology. *Nucleic Acids Res.* 2015;43:8627–8637.
- Henderson A, Wu YL, Huang YC, et al. Lansdorp, Detection of G-quadruplex DNA in

- mammalian cells. *Nucleic Acids Res.* 2014;42:860–869.
- Murat P, Balasubramanian S. Existence and consequences of G-quadruplex structures in DNA. *Curr Opin Genet Dev.* 2014;25:22–29.
 - Gellert M, Lipsett MN, Davies DR. Helix formation by guanylic acid. *PNAS.* 1962;48:2013–2018.
 - Burge S, Parkinson GN, Hazel P, Todd AK, Neidle S. Quadruplex DNA: Sequence, topology and structure. *Nucleic Acids Res.* 2006;34:5402–5415.
 - Mendoza O, Bourdoncle A, Boule JB, Brosh RM, Mergny JL. G-quadruplexes and helicases. *Nucleic Acids Res.* 2016;44:1989–2006.
 - Stegle O, Payet L, Mergny JL, MacKay DC, Huppert JL. Predicting and understanding the stability of G-quadruplexes. *Bioinformatics.* 2009;25:374–382.
 - Tian T, Chen YQ, Wang SR, Zhou X. G-quadruplex: a regulator of gene expression and its chemical targeting. *Chemistry.* 2018;4:1314–1344.
 - Kuzmova E. The Role of G-quadruplexes in Transcriptional Regulation. *Chem Listy.* 2019;113:320–327.
 - C. Monsen, Robert, Trent, O. John. G-quadruplex virtual drug screening: A review, *Biochimie*, 152; 2018:134-148.
 - Schaffitzel C, Berger I, Postberg J, Hanes J, Lipps HJ, Pluckthun A. In vitro generated antibodies specific for telomeric guanine-quadruplex DNA react with *Stylochyta lemnae* macronuclei. *PNAS.* 2001;98:8572–8577.
 - Liu M, Liu Y, Wu F, Du Y, Zhou X. Specific stabilization of DNA G-quadruplex structures with a chemically modified complementary probe. *Bioorg Med Chem.* 2019;27:1962–1965.
 - Duan N, Gong W, Wu S, Wang Z. Selection and Application of ssDNA Aptamers against Clenbuterol Hydrochloride Based on ssDNA Library Immobilized SELEX. *J Agr Food Chem.* 2017;65:1771–1777.
 - Pan W, Zhao J, Chen Q. Fabricating Upconversion Fluorescent Probes for Rapidly Sensing Foodborne Pathogens. *J Agr Food Chem.* 2015;63:8068–8074.
 - Zhang J, Chai X, He X-P, Kim H-J, Yoon J, Tian H. Fluorogenic probes for disease-relevant enzymes. *Chem Soc Rev.* 2019;48:683–722.
 - Long L, Cao S, Jin B, Yuan X, Han Y, Wang K. Construction of a Novel Fluorescent Probe for On-site Measuring Hydrogen Sulfide Levels in Food Samples. *Food Anal Method.* 2019;12:852–858.
 - Liu HW, Chen LL, Xu CY, et al. Recent progresses in small-molecule enzymatic fluorescent probes for cancer imaging. *Chem Soc Rev.* 2018;47:7140–7180.
 - Dhamodharan V, Pradeepkumar P. Specific Recognition of Promoter G-Quadruplex DNAs by Small Molecule Ligands and Light-up Probes. *ACS Chem Biol.* 2019;14:2102–2114.
 - Pandith A, Siddappa RG, Seo YJ. Recent developments in novel blue/green/red/NIR small fluorescent probes for in cellulo tracking of RNA/DNA G-quadruplexes. *J Photoch Photobio C.* 2019;40:81–116.
 - Yuan, J.-H. Shao, W. Chen, S.-B., Huang Z.-S., Tan, J.-H. Recent advances in fluorescent probes for G-quadruplex nucleic acids, *Biochem. Bioph. Res. Co.* In press; 2020.
 - Ma DL, Zhang ZH, Wang MD, Lu LH, Zhong HJ, Leung CH. Recent Developments in G-Quadruplex Probes. *Chem Biol.* 2015;22:812–828.
 - Manna S, Srivatsan SG. Fluorescence-based tools to probe G-quadruplexes in cell-free and cellular environments. *RSC Adv.* 2018;8:25673–25694.
 - Zhang P-L, Wang Z-K, Chen Q-Y, Du X, Gao J. Biocompatible G-Quadruplex/BODIPY assembly for cancer cell imaging and the attenuation of mitochondria. *Bioorg Med Chem Lett.* 2019;29:1943–1947.
 - Chang CC, Kuo IC, Ling IF, et al. Detection quadruplex DNA structures human telomeres fluorescent carbazole derivative. *Anal Chem.* 2004;76:4490–4494.
 - Gao FL, Cao SH, Sun W, Long SR, Fan JL, Peng XJ. Development of a two-photon carbazole derivative probe for fluorescent visualization of G-quadruplex DNA in cells. *Dyes Pigments.* 2019;171.
 - Lu Y-J, Deng Q, Hou J-Q, et al. Molecular Engineering of Thiazole Orange Dye: Change of Fluorescent Signaling from Universal to Specific upon Binding with Nucleic Acids in Bioassay. *ACS Chem Biol.* 2016;11:1019–1029.
 - Wei Y, Zhang X, Wang L, et al. Interaction of bisbenzimidazole-substituted carbazole derivatives with G-quadruplexes and living cells. *RSC Adv.* 2015;5:75911–75917.
 - Lin D, Fei X, Gu Y, et al. A benzindole substituted carbazole cyanine dye: A novel targeting fluorescent probe for parallel c-myc G-quadruplexes. *Analyst.* 2015;140:5772–5780.
 - Hao GY, Sun JY, Wei CY. Studies on interactions of carbazole derivatives with DNA, cell image, and cytotoxicity. *Bioorg Med Chem.* 2018;26:285–294.
 - Wang M-Q, Ren G-Y, Zhao S, et al. Development of a carbazole-based fluorescence probe for G-quadruplex DNA: The importance of side-group effect on binding specificity. *Spectrochim Acta A.* 2018;199:441–447.
 - Li J, Cui Y-C, Bi C-X, et al. Oligo(ethylene glycol)-Functionalized Ratiometric Fluorescent Probe for the Detection of Hydrazine In Vitro and In Vivo. *Anal Chem.* 2019;91:7360–7365.
 - Wang M-Q, Xu J, Zhang L, et al. Tuning the selectivity of N-alkylated styrylquinolinium dyes for sensing of G-quadruplex DNA. *Bioorg Med Chem.* 2019;27:552–559.
 - Wang M-Q, Liao Y-F, Zhang S-H, Yu Q-Q, Huang J-Q. Synthesis, G-Quadruplex DNA binding and cytotoxic properties of naphthalimide substituted styryl dyes. *Bioorg Med Chem.* 2020;51:115325.
 - Divya KP, Sreejith S, Ashokkumar P, et al. A ratiometric fluorescent molecular probe with enhanced two-photon response upon Zn^{2+} binding for in vitro and in vivo bioimaging. *Chem Sci.* 2014;5:3469–3474.
 - Wang M-Q, Zhang Y, Zeng X-Y, et al. A benzo(f)quinolinium fused chromophore-based fluorescent probe for selective detection of c-myc G-Quadruplex DNA with a red emission and a large Stokes shift. *Dyes Pigments.* 2019;168:334–340.
 - Stootman FH, Fisher DM, Rodger A, Aldrich-Wright JR. Improved curve fitting procedures to determine equilibrium binding constants. *Analyst.* 2006;131:1145–1151.
 - Shortreed M, Kopelman R, Kuhn M, Hoyland B. Fluorescent fiber-optic calcium sensor for physiological measurements. *Anal Chem.* 1996;68:1414–1418.
 - Cheng XH, Liu XJ, Bing T, Cao ZH, Shanguan DH. General peroxidase activity of G-Quadruplex-hemin complexes and its application in ligand screening. *Biochemistry.* 2009;48:7817–7823.
 - Lu J, Wang J, Hu X, et al. Electrochemical Biosensor Based on Tetrahedral DNA Nanostructures and G-Quadruplex-Hemin Conformation for the Itrasensitive Detection of MicroRNA-21 in Serum. *Anal Chem.* 2019;91:7353–7359.
 - Trott O, Olson AJ. Software News and Update AutoDock Vina, Improving the Speed and Accuracy of Docking with a New Scoring Function, Efficient Optimization, and Multithreading. *J Comput Chem.* 2010;31:455–461.
 - Jiang MZ, Yan H, He RH, Ma YK. Purification and a molecular docking study of α -glucosidase-inhibitory peptides from a soybean protein hydrolysate with ultrasonic pretreatment. *Eur Food Res Technol.* 2018;244:1995–2005.
 - Barbieri CM, Srinivasan AR, Rzuczek SG, Rice JE, LaVoie EJ, Pilch DS. Defining the mode, energetics and specificity with which a macrocyclic hexaoxazole binds to human telomeric G-quadruplex DNA. *Nucleic Acids Res.* 2007;35:3272–3286.